Ionics (2019) 25:5249–5258
https://doi.org/10.1007/s11581-019-03095-1

ORIGINAL PAPER

Core-shell structure $LiNi_{1/3}Mn_{1/3}Co_{1/3}O_2$@ ultrathin δ-$MnO_2$ nanoflakes cathode material with high electrochemical performance for lithium-ion batteries

Gang Sun[1] · Chenxiao Jia[1] · Jianning Zhang[1] · Liyin Hou[1] · Zhipeng Ma[1] · Guangjie Shao[1] · Zhen-bo Wang[2]

Received: 3 May 2019 / Revised: 10 May 2019 / Accepted: 25 May 2019 / Published online: 14 June 2019

Abstract

Due to the high energy density and low cost, $LiNi_{1/3}Co_{1/3}Mn_{1/3}O_2$ is wildly explored as a promising cathode material for lithium-ion batteries. However, this material suffers from the destruction of surface structure in the electrolyte and the reacting of electrode with the electrolyte during cycles in highly voltage. Herein, we rationally designed core-shell nanostructure $LiNi_{1/3}Mn_{1/3}Co_{1/3}O_2$@ ultrathin δ-$MnO_2$ nanoflakes cathode material with excellent capacity retention and rate capacity by a liquid-phase precipitation method. The unique ultrathin δ-MnO_2 nanoflakes shell nanostructure plays a key role in effectively improving rate performance and cycle life of $LiNi_{1/3}Co_{1/3}Mn_{1/3}O_2$. The electrode with the coating amount of 3 wt% exhibits excellent cycle performance and superior rate capacity compared with bare electrode. The δ-MnO_2 nanoflakes-coated layer can react with Li^+ during cycling and convert to spinel phase, resulting in a reversibly de/lithiation coating layer to improve its specific capacity compared with other inactive coating layer, and the spinel phase can also provide a three-dimensional lithium ions diffusion channels and thus promote lithium ions diffusion. Judging from the discussion, it can be concluded that the role of δ-MnO_2-nanoflakes coating layer not only acts as a protective layer to impede the electrode directly contact with electrolyte but also accelerates lithium ions diffusion and improve its specific capacity.

Keywords Cathode materials · Ultrathin δ-MnO_2 nanosheets · Core-shell nanostructures · Lithium-ion batteries

Introduction

Owing to the consumption of fossil fuels, the release of large quantities of greenhouse gas, especially CO_2, to the atmosphere results in serious environmental hazards [1, 2]. The alternative sustainable energy and clean sources are in high eager to meet the ever-growing energy for use in power battery field or energy storage battery field [3–11]. Lithium-ion batteries (LIBs) are being intensively studied as an energy storage device for electronic products due to its long cycle life and considerable energy density. In the last 20 years, the most widely commercialized cathode materials for LIBs, $LiCoO_2$, have its inherent shortcomings that the only 50% of Li^+ in $LiCoO_2$ can reversible used for its electrochemical performance, and that ultimately limits its storage capacity [12–14]. Recently, many researchers have turned their research focus to layered transition metal oxide ($Li[Ni_xCo_yMn_z]O_2$, NCM, or NCM_{xyz}) cathode materials, which have high practical capacity, low cost, and low toxicity than $LiCoO_2$ [15, 16]. Among the layered $Li[Ni_xCo_yMn_z]O_2$ family, $LiNi_{1/3}Co_{1/3}Mn_{1/3}O_2$ (NCM) has aroused extensive attention owing to the superior cycle life and rate capacity [17, 18].

However, the use of NCM exhibits several limitations since those materials have its inherent shortcomings, including

Gang Sun and Chenxiao Jia contributed equally to this work.

Electronic supplementary material The online version of this article (https://doi.org/10.1007/s11581-019-03095-1) contains supplementary material, which is available to authorized users.

✉ Guangjie Shao
shaoguangjie@ysu.edu.cn

✉ Zhen-bo Wang
wangzhb@hit.edu.cn

[1] College of Environmental and Chemical Engineering, State key Laboratory of Metastable Materials Science and Technology, Yanshan University, Qinhuangdao 066004, China

[2] MIIT Key Laboratory of Critical Materials Technology for New Energy Conversion and Storage, School of Chemistry and Chemical Engineering, Harbin Institute of Technology, Harbin 150001, China

rapid practical capacity attenuation during long cycling and poor Li^+ diffusion, especially in highly overcharged [19–21]. These drawbacks may be a result of [22–26]: (1) the dissolution of transition metal ions (Ni, Mn, Co) in electrolytes due to the reacting of cathode materials with the electrolyte; (2) structural instability because the transition metal (TM) ions (Ni^{2+}, 0.69 Å, similar to the ionic radius of Li^+, 0.76 Å) may migrate from TM sites in TM-layer into Li^+ vacant sites in Li-layer at highly delithiated state; (3) instability plague the electrodes, electrolytes, and their interfaces and surface impedance increased (the formation of a solid electrolyte interphase (SEI) layer). It is critical to develop a stable interfacial layer on the electrodes and electrolytes for achieving a long cycle performance, as degradation is typically originated from the encounter between the electrode and the electrolyte. Various surface modifications have been investigated to develop a stable interfacial layer, which could enhance the electrochemical performance of the cathode materials. For example, inorganic compounds such as metal oxides (Nb_2O_5 [27], Sb_2O_3 [28], TiO_2 [29], ZrO_2 [30], and Al_2O_3 [31, 32]), fluorides (AlF_3 [33]), carbon [34], and phosphates ($AlPO_4$ [35]) have been coated onto $LiNi_{1-x-y}Co_xMn_yO_2$ to improve the structural stability. Su et al. [36] reported an atomic layer-deposited (ALD) Al_2O_3 layer coated NCM material cycled in the voltage range of 3.0–4.5 V (high voltage). The results demonstrated that the electrode with ALD Al_2O_3-coated NMC has much enhanced cycling stability, which attributes to the Al_2O_3 layer, as a protective layer, protects the electrode from direct contact and react with electrolyte. However, a thick electrochemical inactive Al_2O_3 coating with high resistive leads to the reversible capacity loss especially at high-C rate [32]. Therefore, the appropriate coating materials and strategies, which can effectively protect the surface of the material from dissolution, as well as provide the conduction channel for the rapid diffusion of lithium ions from the electrode to electrolyte, are in high demanded to efficient enhance the electrochemical performance of NCM. Guo et al. [37] reported a MnO_2-coated NCM cathode material prepared by a chemical deposition method, which shows greatly enhancement of the electrochemical performance especially the rate capability. Electrochemical active oxide MnO_2 has been widely investigated in supercapacitor [38–40], catalytic [41–43], and lithium-ion batteries [44, 45]. It possesses many advantages as a coating layer, such as the high theoretical capacity, earth abundance, low cost, and low toxicity, and different types of MnO_2 can be synthesized by numerous methods. Therefore, it is necessary to have a systematic study of MnO_2 coating layer.

Herein, a novel availably strategy has been proposed to generate the core-shell $LiNi_{1/3}Mn_{1/3}Co_{1/3}O_2$@ ultrathin δ-$MnO_2$ nanoflakes nanostructure materials with ultrahigh rate property and long cycle life via a liquid-phase precipitation method. The optimal temperature of thermal treatment for the δ-MnO_2 nanoflakes-coated NCM samples is 400 °C. The ultrathin δ-MnO_2 nanoflakes-coated electrode with coating amount of 3 wt% exhibits a great cycle performance and superior rate capacity compared with the pristine electrode. The δ-MnO_2 nanosheet-coated layer can react with Li^+ during cycling and convert to spinel phase, resulting in higher discharge capacity of coated electrode, and the spinel phase formed after cycles can also provide a three-dimensional lithium ions diffusion channels and thus promote lithium ions diffusion. Here is the detail discussing its prepared method and electrochemical behavior.

Experimental section

Materials preparation and characterization

The ultrathin δ-MnO_2 nanoflakes are prepared by chemical precipitation method as our previously reported [38]. Typically, a certain amount of manganese acetate acid were dispersed in distilled water and treated by ultrasound. Follow on the proper amount of ethylenediaminetetraacetic acid disodium salt (EDTA) and sodium dodecyl sulfonate (SDS) that were added into the above mixed solution under vigorous stirring at 30 °C. Then, NaOH aqueous solution was added drop by drop to the above mixed solution. And $K_2S_2O_8$ aqueous solution was added drop by drop to initiate the chemical deposition reaction. The above suspension liquid was kept for 12 h under water bath at 30 °C. The obtained powders were calcined at 300 °C, 400 °C, 500 °C, and 600 °C for 2 h in air at a rate of 2 °C min^{-1} to obtain ultrathin δ-MnO_2 nanoflakes. The obtained compound was named as MnO_2–300 °C, MnO_2–400 °C, MnO_2–500 °C, and MnO_2–600 °C, respectively. The obtained compound without any thermal treatment was named as MnO_2–25 °C.

Core-shell $LiNi_{1/3}Mn_{1/3}Co_{1/3}O_2$@ ultrathin δ-$MnO_2$ nanoflakes nanostructure materials with superior rate capacity and cycle performance were synthesized via a chemical bath deposition. Pristine $LiNi_{1/3}Mn_{1/3}Co_{1/3}O_2$ named as NCM was provided by the 18th Research Institute Of China Electronics Technology Group Corporation. Typically, the pristine $LiNi_{1/3}Mn_{1/3}Co_{1/3}O_2$ was dispersed in distilled water and ultrasound for a period of time, and manganese acetate acid were dispersed in the above solution and sonicated for 30 min. And then core-shell $LiNi_{1/3}Mn_{1/3}Co_{1/3}O_2$@ ultrathin δ-$MnO_2$ nanoflakes nanostructures were prepared according to the above procedure without any thermal treatment. The obtained $LiNi_{1/3}Mn_{1/3}Co_{1/3}O_2$@ ultrathin δ-$MnO_2$ nanoflakes with different coating amount of 1 wt%, 2 wt%, 3 wt%, 4 wt%, and 5 wt% were synthesized by controlling different reaction conditions.

The 3 wt% δ-MnO_2-coated $LiNi_{1/3}Mn_{1/3}Co_{1/3}O_2$ without any thermally treatment was named as M-25 °C. And the samples of 3 wt% δ-MnO_2-coated $LiNi_{1/3}Mn_{1/3}Co_{1/3}O_2$,

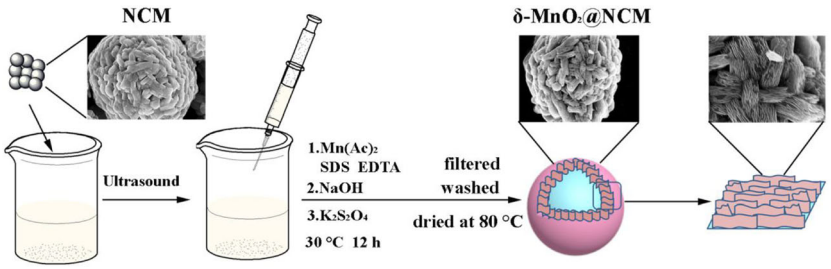

Fig. 1 Fabrication process of the $LiNi_{1/3}Mn_{1/3}Co_{1/3}O_2$@ultrathin δ-$MnO_2$ nanosheets core-shell structure

which were calcined at 300 °C, 400 °C, and 500 °C for 2 h in air at a rate of 2 °C min^{-1}, were named as M-300 °C, M-400 °C, and M-500 °C, respectively.

Finally, the above $LiNi_{1/3}Mn_{1/3}Co_{1/3}O_2$@ ultrathin δ-$MnO_2$ nanosheets with different coating amounts of 1 wt%, 2 wt%, 3 wt%, 4 wt%, and 5 wt% were thermal treatment at 400 °C for 2 h in air at a rate of 2 °C min^{-1} and were named as S-1, S-2, S-3, S-4, and S-5, respectively. The M-400 °C and S-3 are the same sample. The schematic illustration of the synthetic process is displayed in Fig. 1.

The crystal structure of as-prepared samples was conducted on XRD (X-ray diffraction operated at 40 kV using a Cu Kα (λ = 1.5406 Å) radiation) at a scanning rate of 5° min^{-1} between 10° and 80° (2 θ). The morphology and microstructure of the powders were characterized on a SEM (scanning electron microscopy, Carl Zeiss Super55 operated at 5 kV) and TEM (emission transmission electron microscope, Hitachi HT7700 operated at 120 kV).

Electrochemical measurements

The prepared electrodes mainly contain 3 parts: (1) the active material (as-prepared samples, 80 wt%); (2) conductive additive (carbon black, 10 wt%); (3) binding agent (polyvinylidene fluoride, 10 wt%). The above mixed materials were dispersed in N-methyl pyrrolidone and then uniformly casting the slurry onto the Al foil and dried in a vacuum at 120 °C for 12 h. The average mass loading of active materials

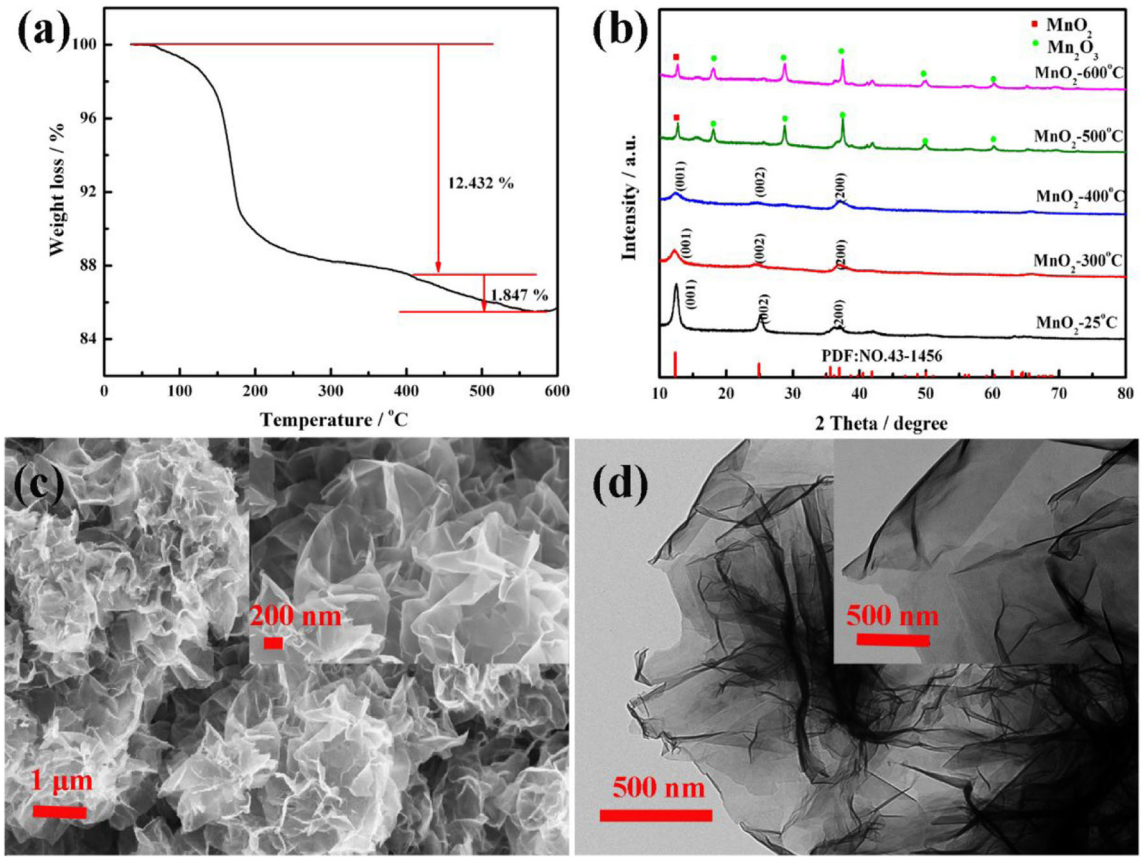

Fig. 2 **a** TGA results of δ-MnO_2 nanosheets. **b** XRD patterns of δ-MnO_2 nanosheets at different thermally treatment. SEM images (**c**) and TEM images (**d**) of the ultrathin δ-MnO_2 nanosheets

on the electrode is about 3.2 mg cm^{-2}. Coin cells were assembled to measured electrochemical performance with fresh Li foil as the counter electrode, a microporous polypropylene film (Celgard 2400) as the separator, and a solution of 1 M $LiPF_6$ in a mixture of ethylene carbonate and diethyl carbonate with 1:1 volume ratio as the electrolyte in an Ar-filled glove box.

The electrochemical performance was tested on a LAND battery testing system (Wuhan, China) by galvanostatic charge/discharge cycling between 2.50 and 4.50 V (vs Li + /Li) at 25 °C. The current density of 200 mA g^{-1} is equal to the 1 C rate at voltage range of 2.50 to 4.50 V. Electrochemical impedance spectroscopy (EIS) was measured on a CHI660E electrochemical workstation (Chenhua, Shanghai, China) over an alternating current frequency range of 100 kHz to 0.01 Hz.

Result and discussion

The ultrathin δ-MnO_2 nanosheets can be obtained by chemical precipitation method. According to the report in the previous literature [46], the water content will seriously affect the conductivity of MnO_2. Usually, the conductivity of MnO_2 is inversely proportional to the water content. The electrical conductivity of MnO_2 can be improved with the decrease of its moisture content. Furthermore, the presence of moisture has a very adverse effect on the performance of lithium-ion batteries. In this work, MnO_2 is required to have a high conductivity, which can be conducive to the rapid conduction of lithium ions. Therefore, it is very crucial to control the temperature of the heat treatment of the sample. The TGA result of δ-MnO_2 nanosheets is shown in Fig. 1a. There is 12.4% of the weight loss of the δ-MnO_2 nanoflakes around 400 °C, owing to the remove of the adsorbed water and crystal water of MnO_2 [43, 47]. The weight loss of the δ-MnO_2 nanosheets is about 1.8%, when the temperature subsequently goes up to 600 °C, due to the changes in the structure of δ-MnO_2, gradually changing to Mn_2O_3. The crystal structure of δ-MnO_2 nanoflakes at different thermally treatment temperatures were investigated by XRD (Fig. 2b). Apparently, the diffraction peaks of the MnO_2–25 °C, MnO_2–300 °C, and MnO_2–400 °C samples (shown in Fig. 2b) can be well indexed as pure δ-phase MnO_2 (JCPDS card no. 43-1456) phase without any impurity peaks. The intensity of the diffraction peaks of the δ-phase MnO_2 decreased with the temperature of thermally treatment increased before 400 °C which means the decline in crystalline, which is mainly because the process of dehydration reduces the crystallinity of the material. But the conductivity of the material increases with the temperature increased to 400 °C as the above discussion. It can be obviously observed that those minor impurity peaks regarding Mn_2O_3 appear in the pattern of MnO_2–500 °C and MnO_2–600 °C that mainly because of the MnO_2 is converted to Mn_2O_3 after 400 °C. The XRD results are corresponding to the TGA result. However, the poor conductivity of Mn_2O_3 means that it is not a potential coating layer. In addition, considering that the electrode material of the battery is required to completely remove adsorbed water and bound water in the MnO_2, therefore, it can be predicted that the optimal temperature of thermal treatment is 400 °C. The SEM image and TEM image of the pristine δ-MnO_2 nanoflakes obtained by chemical bath deposition, and a magnified SEM image and TEM image obtained in Fig. 2c, d. The nanoflakes displays ample graphene-like wrinkles and folds with ultrathin and lamellar structures. Furthermore, the ultrathin δ-MnO_2 nanoflakes with lateral size of several micrometers are interwoven with each other. That structure cloud shorter the lithium ion diffusion path, and more conducive to increases the area which can prove more Li^+ diffusion channel between the electrode and the electrolyte, and makes Li^+ diffusion becomes easier.

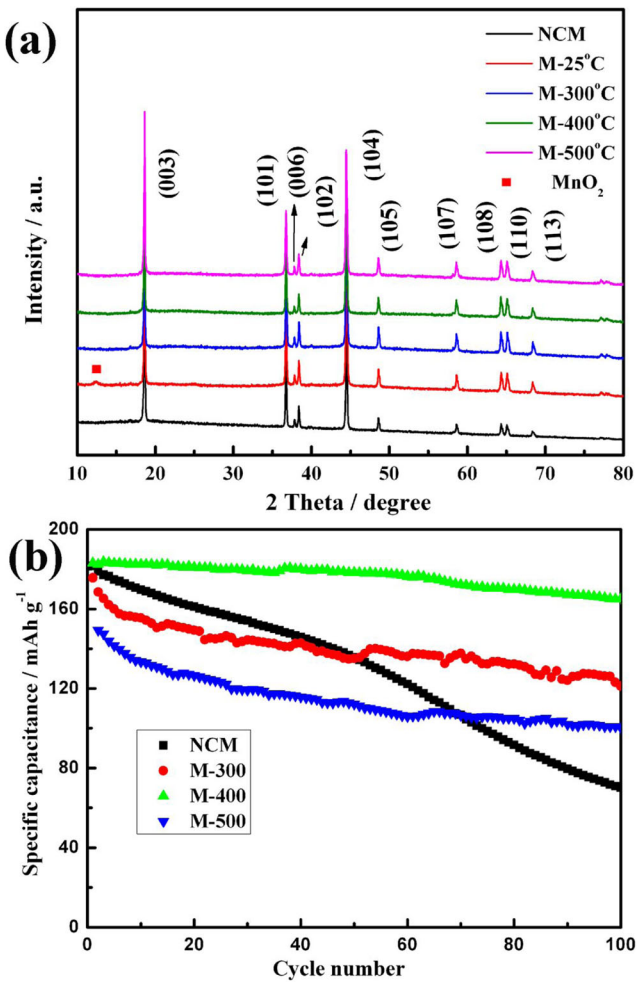

Fig. 3 **a** XRD patterns of $LiNi_{1/3}Mn_{1/3}Co_{1/3}O_2$@ultrathin δ-$MnO_2$ nanosheets at different thermally treatment. **b** Cycling performance for NCM, M-300, M-400, and M-500 electrodes under a current rate of 1 C. All measurements are conducted in the voltage range of 2.5–4.5 V vs Li/Li^+

The XRD patterns of $LiNi_{1/3}Mn_{1/3}Co_{1/3}O_2$@ ultrathin δ-$MnO_2$ nanoflakes at different thermally treatment temperature were illustrated in Fig. 3a. All Bragg peaks of as-prepared samples shown in XRD patterns could be indexed on a rhombohedral phase with the pace group R-3 m. What's more, no impurity phases could be found after modified treatment due to the low content of δ-MnO_2 coating. All samples exhibit an ordered layered structure, based on the well splitting of hexagonal doublets (006)/(012) and (018)/(110) peaks [1, 48]. What's more, no significant difference can be observed in Fig. 3a in the XRD patterns before and after the δ-MnO_2 coating, indicating no significant change happened in the layered structure of $LiNi_{1/3}Mn_{1/3}Co_{1/3}O_2$ after the coating. Some minor impurity peaks appear in the M-25 °C sample mainly due to larger content of crystal water contained in δ-MnO_2, which has a negative impact for the performance of lithium-ion battery. Figure 3b shows that the cycling performance for NCM, M-300 °C, M-400 °C, and M-500 °C electrodes at 1 C between 2.50 and 4.50 V vs Li/Li^+. There is no capacity of M-25 °C due to larger water content. The specific discharge capacities on first cycle of the NCM, M-300 °C, M-400 °C, and M-500 °C electrodes were found to be 181.6, 175.7, 183.0, and 149.3 mAh g^{-1}, respectively. As what we talk above, the M-300 °C sample has poor lithium ion conductivity mainly because the crystal water contained in δ-MnO_2 has not been completely removed, as well as when the temperature of thermally treatment goes to 500 °C, MnO_2 is converted to Mn_2O_3 decreased the conductivity of the coating layer. That is all results in lower initial specific capacities of M-300 °C and M-500 °C electrodes than the pristine NCM electrode. The capacity retentions of the NCM, M-300 °C, M-400 °C, and M-500 °C electrodes are 38.6%, 69.0%, 90.2%, and 66.7% over 100 cycles, respectively. Obviously, the M-400 °C electrode exhibits the highest capacity retention ratio after 100 cycles. The results indicate the optimal temperature of thermal treatment is 400 °C, which is consistent with what we discussed earlier.

In order to rationally design core-shell $LiNi_{1/3}Mn_{1/3}Co_{1/3}O_2$@ ultrathin δ-$MnO_2$ nanoflakes structure, different amount of δ-

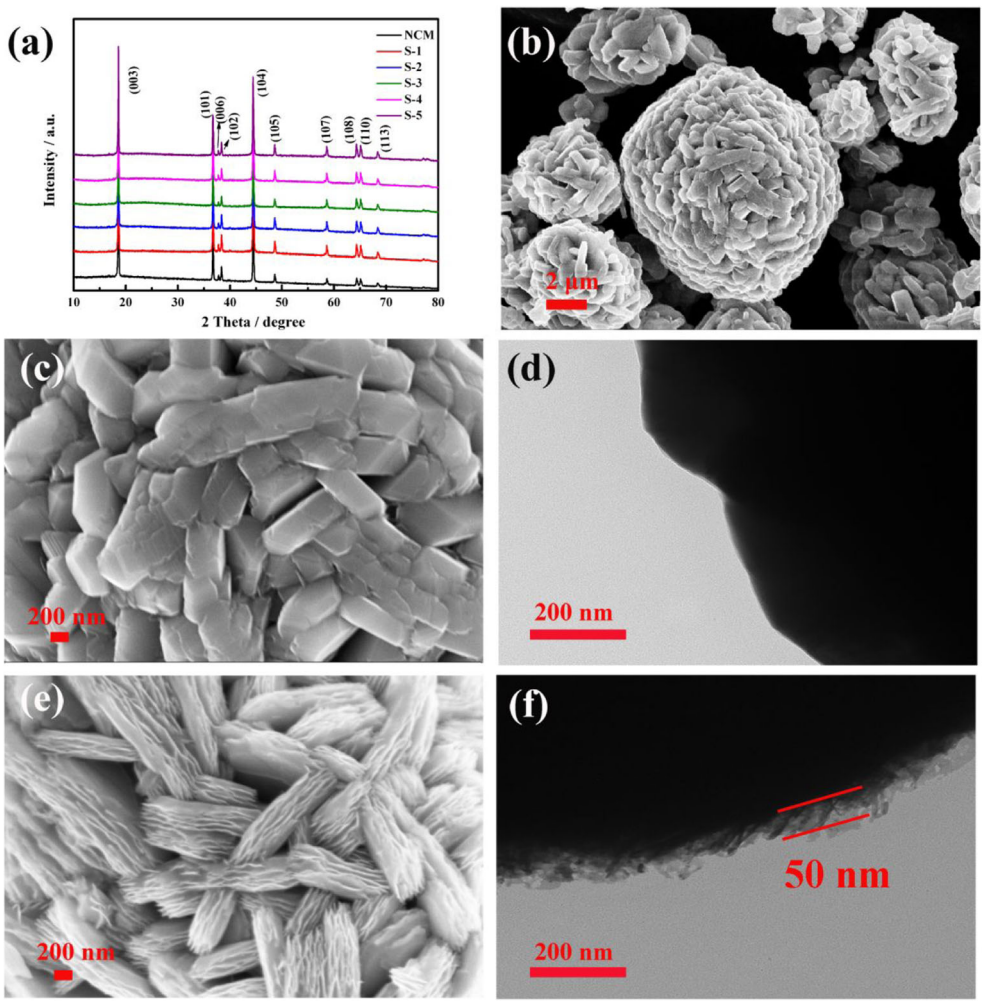

Fig. 4 XRD patterns of $LiNi_{1/3}Mn_{1/3}Co_{1/3}O_2$@ultrathin δ-$MnO_2$ nanosheets (**a**) with different coating amount. **b**, **c** SEM images of NCM under different magnification scans, TEM images (**d**) of NCM. SEM images (**e**) and TEM images (**f**) of S-3

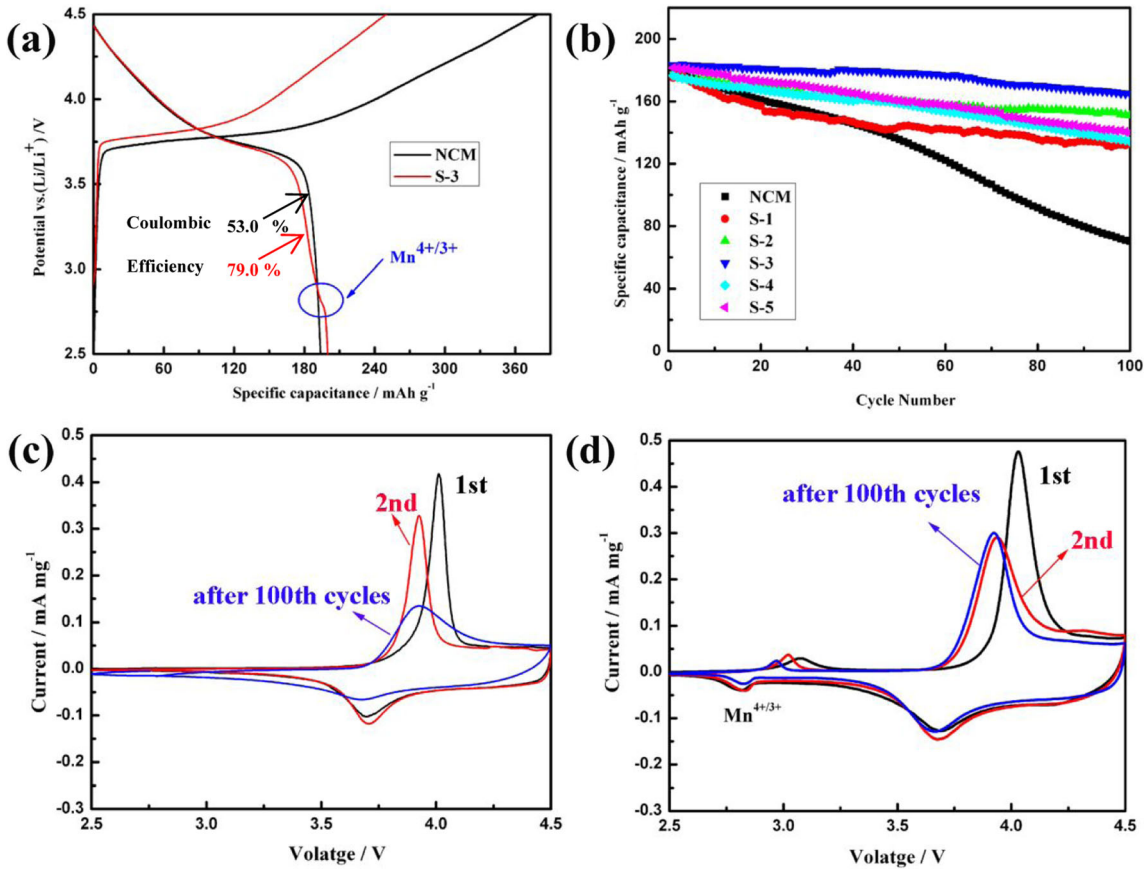

Fig. 5 **a** Initial charge and discharge curves of NCM and S-3 samples under a current rate of 0.2 C. **b** Cycling performance for NCM, S-1, S-2, S-3, S-4, and L-5 electrodes under a current rate of 1 C; cyclic voltammograms for NCM (**c**) and S-3 (**d**) samples before and after 100th cycles at a scan rate of 0.1 mV s^{-1} at 25 °C. All measurements are conducted in the voltage range of 2.5–4.5 V vs Li/Li^+

MnO_2 coated on NCM were synthesized. The XRD patterns of $LiNi_{1/3}Mn_{1/3}Co_{1/3}O_2$@ ultrathin δ-$MnO_2$ nanoflakes with different coating amounts are displayed in Fig. 4a. There is no significant difference in the crystal structure after different amount of δ-MnO_2 coating too, which is corresponding to the above discussion. Meanwhile, $I_{(003)/(104)}$ (I corresponding to the peak intensity ratio) is applied to reflects the degree of cation mixing, and the value larger than 1.2 indicates that the cation Ni^{2+} and Li^+ exhibit great ordering in layer structure [20]. The $I_{(003)/(104)}$ ratios of pristine NCM, S-1, S-2, S-3, S-4, and S-5 are 1.138, 1.240, 1.414, 1.526, 1.335, and 1.277 respectively. The intensity ratio of the (003) and (104) peaks for coating samples is larger than 1.2, which also means the better cation ordering of coating samples. The largest value of I(003)/I(104) for S-3 indicates lower cation mixing than other samples, which may benefit for diffusion of lithium ions. Meanwhile, SEM and TEM were used to analyze the surface morphologies and microstructures of bare and the δ-MnO_2 coated on NCM samples to explore the influence of the coating layer on surface morphology. The morphologies of the as-synthesized NCM, S-1, S-2, S-3, S-4, and S-5 powders are shown in Fig. 4b–f and Fig. S1. The NCM particles are assembled from rod-shaped primary particles, and the size of the particle is about 10 μm, which can be seen in Fig. 4b. The SEM and TEM images of the NCM and S-3 particles were shown in Fig. 4c–f. With a particle size of 1 to 2 μm, the primary particle of NCM displays a clear boundary and smooth surface, while the modified $LiNi_{1/3}Mn_{1/3}Co_{1/3}O_2$ is distinctly covered by δ-MnO_2 nanosheets. The S-3 sample exhibits a uniform array of δ-MnO_2 nanosheets coating layer on the

Table 1 Cycle performance of the prepared samples at 1 C in the voltage range of 2.5–4.5 V

	1st discharge capacity (mA h g^{-1})	100th discharge capacity (mA h g^{-1})	100th capacity retention (%)
NCM	181.6	70.2	38.6
S-1	175.1	132.6	75.7
S-2	177.7	151.1	85.0
S-3	183.4	165.0	90.2
S-4	176.4	134.3	76.1
S-5	181.4	140.1	77.23

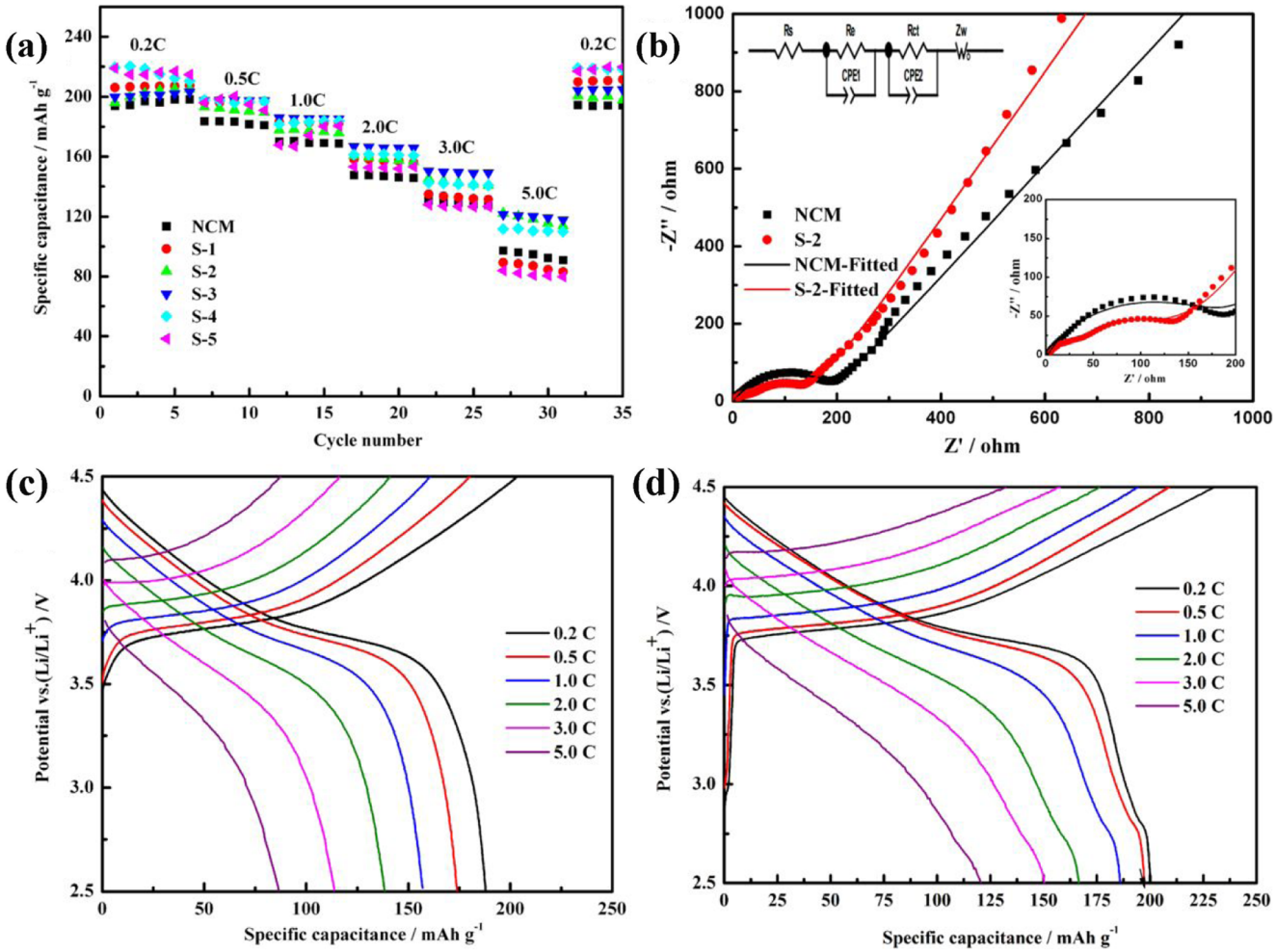

Fig. 6 **a** Rate capability tests at several currents (C rates) for NCM, S-1, S-2, S-3, S-4, and L-5 electrodes in the potential range of 2.5–4.5 V versus Li. **b** Nyquist plots for the NCM and S-3 electrodes after the 100th cycling, with the equivalent circuit as the inset; discharge profiles of NCM (**c**) and S-3 (**d**) electrodes cathode at various C rates of 0.2, 0.5, 1, 2, 3, and 5 C

surface of NCM particles, which is conductive to the infiltration of electrolyte and the diffusion of lithium ions. The SEM and TEM images of S-1, S-2, S-4, and S-5 samples are shown Fig. S1. An uncontinuously δ-MnO_2 coating layer was deposited on the surface of NCM particles, and making part of the NCM particles exposed to the electrolyte, which may due to the small coating amount and uneven dispersion. With the increase of the coating amount, the coating layer on the surface of the particles become rough and dense, and this will adversely affect the wetting of the electrolyte, resulting in a poor electrochemistry performance.

The electrochemical performance was tested by galvanostatic charge/discharge cycling between 2.50 and 4.50 V (vs Li^+/Li) at 25 °C to compare cycle life of bare and coated samples. The initial charge/discharge capacity profiles and first coulombic efficiency of the pristine NCM and S-3 at 0.2 C in the potential range of 2.5–4.5 V were presented in Fig. 5a. The initial coulombic efficiency of S-3 is 79.9% compared 53.0% for bare NCM samples, which has been greatly improved by the coating of δ-MnO_2 nanoflakes on NCM. Notably, a small platform emerged at about 2.8 V due to Li^+ inserted to the δ-MnO_2 nanoflakes layer in the discharge process, delivered more discharge capacities. The pristine NCM electrode exhibits a discharge capacity of 193.8 mAh g^{-1}, whereas the δ-MnO_2 nanoflakes-coated electrode displays a discharge capacity of 199.9 mAh g^{-1}. The cycling performances of the bare NCM and ultrathin δ-MnO_2 nanoflakes coated NCM with different coating amounts at current rate of 1 C between 2.50 and 4.5 V are presented in Fig. 5b and Table 1. The discharge capacity of NCM electrode decreases to 70.2 mAh g^{-1} after 100 cycles,

Table 2 Electrochemical impedance of the NCM and S-3 electrodes

Sample	Rs (Ω)	Re (Ω)	Rct (Ω)
NCM	2.556	13.19	149.6
S-3	0.93	20.04	43.97

corresponding to 38.6% capacity retention. Compared to the pristine electrode, the ultrathin δ-MnO_2 nanosheets coated NCM displays capacity retention rate of 75.7%, 85.0%, 90.2%, 76.13%, and 77.2% for S-1, S-2, S-3, S-4, and S-5 electrodes after 100 cycles, corresponding to discharge capacities of 132.6, 151.1, 165.0, 134.3, and 140.1 mAh g^{-1}, respectively. The degradation of surface structure and decomposition of electrolyte (high reactive Ni^{4+}, Mn^{4+} dissolution, and/or lithium residual species) result in the rapid capacity fading of pristine electrode. The enhanced cycling performance for coated electrodes is principally associated with the ultrathin δ-MnO_2 nanoflakes layer that separate the electrode surface from directly contacting with electrolyte and eventually impede the interfacial side reactions. Easy to find from the above results, the S-3 electrode exhibits the best cycle performance at 1 C, which is mainly due to the uniform array of δ-MnO_2 nanoflakes coating layer, improving the infiltration of electrolyte and the diffusion of Li^+, and meanwhile reduces the side reactions between the electrode and electrolyte. Cyclic voltammograms for NCM (c) and S-3 (d) samples before and after 100th cycles at a scan rate of 0.1 mV s^{-1} at 25 °C was performed to confirm the effectiveness of δ-MnO_2 nanosheets coating layer and the results are presented in Fig. 5c, d, respectively. The first scan and the second one of the CV profiles for the coated and uncoated electrodes exhibit a great difference, due to the large over potential and high electrochemical polarization in the first cycle [49]. The CV peak at about 3.9 V for the NCM and S-3 electrode is corresponding to the redox couples of Ni^{2+}/Ni^{4+}. Besides, as for δ-MnO_2 nanoflakes-coated electrode, the CV peak at low voltage around 2.8 V, belonging to redox couples of $Mn^{3+/4+}$, can be attributed to the process of de/lithiation in δ-MnO_2 during charging and discharging. Similar peak at 2.84 V in the previous works is usually linked to the spinel phase [50, 51]. This result is well consistent with what we talk about in the charge/discharge profiles. Lithium ions are embedded in the δ-MnO_2 layer and converts to spinel phase, providing partial capacity, and resulting in higher discharge capacity. Notably, the bare electrode without any treatment exhibits observable capacity fading compared the δ-MnO_2-coated electrode. The CV curves of δ-MnO_2-coated electrode overlap much better compared with the bare cathode, also indicating the superior electrochemical cycle life.

The superior electrochemical cycle stability and specific capacity play a very important role for cathode materials as well as rate capability. The rate capacity of bare and the δ-MnO_2-coated electrodes were illustrated in Fig. 6a. The S-3 electrode demonstrates the best rate capacity. The discharge curves at various rates are shown in Fig. 6c, d. The S-3 electrode delivers 121.5 mAh g^{-1} at 5 C, whereas the bare NCM release 86.9 mAh g^{-1}. The δ-MnO_2-coated electrodes show a batter rate capacity compared the bare electrode. The improvement of rate performance of δ-MnO_2-coated electrode is due to the formed spinel phase after Li embedded in a lattice of δ-MnO_2-coating layer, which can provide a 3D (three-dimensional) Li^+ diffusion channel and promote the diffusion of Li^+. Judging from the discussion above, the role of δ-MnO_2-nanoflakes layer in the cathode materials not only acts as a protective layer to impede the electrode direct contact with the electrolyte but also accelerates the diffusion of Li^+. The Nyquist plots of NCM and S-3 electrode are fitted after 100th cycling in coin cell and presented in Fig. 6b. From the equivalent circuits in the illustration of Fig. 6b, Rs stands for the solution impedance (included the ohmic resistance between working electrode and Li electrode); Re corresponds to the Li^+ diffusion impedance; Rct represents charge transfer through the electrode/electrolyte interface [52]. The fitted values of corresponding impedance after the 100th cycle are displayed in Table 2. The value of Rct of S-3 according to the fitting results is 43.97 Ω compared with 149.6 Ω for NCM, indicating that S-3 sample possesses the great electronic contact and more effective charge transport than NCM, and eventually resulting a higher rate property. From all the above discussion, we can conclude that the δ-MnO_2-nanoflakes layer on the surface of the cathode materials not only acts as a protective layer to impede the electrode directly contact with electrolyte but also accelerates lithium ions diffusion and improves its specific capacity.

Conclusions

Herein, we rationally designed core-shell $LiNi_{1/3}Mn_{1/3}Co_{1/3}O_2$@ ultrathin δ-$MnO_2$ nanoflakes nanostructures materials with great electrochemical cycle life and rate capacity via a chemical bath deposition method. The optimal temperature of thermal treatment for the δ-MnO_2 nanosheets coated $LiNi_{1/3}Mn_{1/3}Co_{1/3}O_2$ sample is 400 °C. Combining electrochemical measurements, the ultrathin δ-MnO_2 nanosheets-coated electrode with the coating amount of 3 wt% exhibits a great cycle performance and superior rate capacity compared with the pristine electrode. It can be demonstrated from the charge/discharge plots and CV curves that the δ-MnO_2 nanosheets coated layer can react with Li^+ during cycling and converts to spinel phase, resulting in the higher specific capacity of coated electrode. The spinel phase formed after cycles coated on the electrode can also provide a 3D Li^+ diffusion channel and then improve the diffusion of Li^+. To sum up, the electrochemical activity δ-MnO_2 nanoflakes can provide more Li^+ insertion/extraction sites, providing extra capacity; meanwhile, the coating layer acts as a protective layer to impede the electrode directly contact with electrolyte to minimize the interface side reactions.

Funding information This work was financially supported by the National Natural Science Foundation of China 51674221 and National Natural Science Foundation of China 51704261 and the Natural Science Foundation of Hebei Province B2018203330 and Natural Science Foundation of Hebei Province B2018203360.

Compliance with ethical standards

Conflict of interest The authors declare that they have no conflict of interest.

References

1. Ibrahim H, Ilinca A, Perron J (2008) Energy storage systems—characteristics and comparisons. Renew Sust Energ Rev 12:1221–1250
2. Aricò AS, Bruce P, Scrosati B, Tarascon JM, Van Schalkwijk W (2005) Nanostructured materials for advanced energy conversion and storage devices. Nat Mater 4:366–377
3. Yuksel I, Kaygusuz K (2011) Renewable energy sources for clean and sustainable energy policies in Turkey. Renew Sust Energ Rev 15:4132–4144
4. Bilgen S, Kaygusuz K, Sari A (2004) Renewable energy for a clean and sustainable future. Energy Sources 26:1119–1129
5. Chen Z, Ma Z, Song J, Wang L, Shao G (2016) Novel one-step synthesis of wool-ball-like Ni-carbon nanotubes composite cathodes with favorable electrocatalytic activity for hydrogen evolution reaction in alkaline solution. J Power Sources 324:86–96
6. Yi T-F, Zhu Y-R, Tao W, Luo S, Xie Y, Li X-F (2018) Recent advances in the research of MLi2Ti6O14 (M= 2Na, Sr, Ba, Pb) anode materials for Li-ion batteries. J Power Sources 399:26–41
7. Han X, Gui X, Yi T-F, Li Y, Yue C (2018) Recent progress of NiCo2O4-based anodes for high-performance lithium-ion batteries. Curr Opinion Solid State Mater Sci 22:109–126
8. Yang W, Yang W, Sun B, Di S, Yan K, Wang G, Shao G (2018) Mixed lithium oxynitride/oxysulfide as an interphase protective layer to stabilize lithium anodes for high-performance lithium–sulfur batteries. ACS Appl Mater Interfaces 10:39695–39704
9. Yang W, Yang W, Dong L, Gao X, Wang G, Shao G (2019) Enabling immobilization and conversion of polysulfides through a nitrogen-doped carbon nanotubes/ultrathin MoS 2 nanosheet core–shell architecture for lithium–sulfur batteries. J Mater Chem A 7:13103–13112
10. Yang W, Yang W, Zhang F, Wang G, Shao G (2018) Hierarchical interconnected expanded graphitic ribbons embedded with amorphous carbon: an advanced carbon nanostructure for superior lithium and sodium storage. Small 14:1802221
11. Song A, Cao L, Yang W, Li Y, Qin X, Shao G (2018) Uniform multilayer graphene-coated iron and iron-carbide as oxygen reduction catalyst. ACS Sustain Chem Eng 6:4890–4898. https://doi.org/10.1021/acssuschemeng.7b04319
12. Whittingham MS (2004) Lithium batteries and cathode materials. Cheminform 35:4271
13. Van EJ, Wieland JL, Eskes H, Kuiper P, Sawatzky GA, de Groot FM, Turner TS (1991) Electronic structure of CoO, Li-doped CoO, and $LiCoO_2$. Phys Rev B Condens Matter 44:6090
14. Auvergniot J, Cassel A, Ledeuil JB, Viallet V, Seznec V, Dedryvère R (2017) Interface stability of argyrodite Li_6PS_5Cl towards $LiCoO_2$, $LiNi_{1/3}Co_{1/3}Mn_{1/3}O_2$ and $LiMn_2O_4$ in bulk all-solid-state batteries. Chem Mater 29:3883–3890
15. Kim D, Shim HC, Yun TG, Hyun S, Han SM (2016) High throughput combinatorial analysis of mechanical and electrochemical properties of $Li[Ni_xCo_yMn_z]O_2$ cathode. Extreme Mech Lett 9:439–448
16. Manthiram A, Song B, Li W (2016) A perspective on nickel-rich layered oxide cathodes for lithium-ion batteries. Energy Storage Mater 6:125–139
17. Lee MH, Kang YJ, Myung ST, Sun YK (2004) Synthetic optimization of $Li[Ni_{1/3}Co_{1/3}Mn_{1/3}]O_2$ via co-precipitation. Electrochim Acta 50:939–948
18. Shaju KM, Bruce PG (2006) Macroporous Li $(Ni_{1/3}Co_{1/3}Mn_{1/3})O_2$: a high-power and high-energy cathode for rechargeable lithium batteries. Adv Mater 18:2330–2334
19. Goodenough JB, Kim Y (2009) Challenges for rechargeable Li batteries. Chem Mater 22:587–603
20. Sun G, Yin X, Yang W, Song A, Jia C, Yang W, Du Q, Ma Z, Shao G (2017) The effect of cation mixing controlled by thermal treatment duration on the electrochemical stability of lithium transition-metal oxides. Phys Chem Chem Phys 19:29886–29894
21. Sun G, Yin X, Yang W, Zhang J, Du Q, Ma Z, Shao G, Wang Z-B (2018) Synergistic effects of ion doping and surface-modifying for lithium transition-metal oxide: synthesis and characterization of La2O3-modified LiNi1/3Co1/3Mn1/3O2. Electrochim Acta 272:11–21
22. Shaju KM, Rao GVS, Chowdari BVR (2004) Influence of Li-ion kinetics in the cathodic performance of layered $Li(Ni_{1/3}Co_{1/3}Mn_{1/3})O_2$. J Electrochem Soc 151:A1324–A1332
23. Luo X, Wang X, Liao L, Wang X, Gamboa S, Sebastian PJ (2006) Effects of synthesis conditions on the structural and electrochemical properties of layered $Li[Ni_{1/3}Co_{1/3}Mn_{1/3}]O_2$ cathode material via the hydroxide co-precipitation method LIB SCITECH. J Power Sources 161:601–605
24. Deb A, Bergmann U, Cramer SP, Cairns EJ (2005) In situ x-ray absorption spectroscopic study of the $Li[Ni_{1\ 3}Co_{1\ 3}Mn_{1\ 3}]O_2$ cathode material. J Appl Phys 97:1
25. Myung S-T, Lee K-S, Yoon C S, Sun Y-K, Amine K, Yashiro H (2010) Effect of AlF_3 coating on thermal behavior of chemically Delithiated $Li_{0.35}[Ni_{1/3}Co_{1/3}Mn_{1/3}]O_2$. J Phys Chem C 114:4710–4718
26. Zheng J, Liu T, Hu Z, Wei Y, Song X, Ren Y, Wang W, Rao M, Lin Y, Chen Z (2016) Tuning of thermal stability in layered $Li(Ni_xMn_yCo_z)O_2$. J Am Chem Soc 138:13326–13334
27. Uchida S, Zettsu N, Hirata K, Kami K, Teshima K (2016) High-voltage capabilities of ultra-thin Nb_2O_5 nanosheet coated $LiNi_{1/3}Co_{1/3}Mn_{1/3}O_2$ cathodes. RSC Adv 6:67514–67519
28. Han Z, Yu J, Zhan H, Liu X, Zhou Y (2014) Sb_2O_3-modified $LiNi_{1/3}Co_{1/3}Mn_{1/3}O_2$ material with enhanced thermal safety and electrochemical property. J Power Sources 254:106–111
29. Zhang Y, Wang Z-B, Yu F-D, Que L-F, Wang M-J, Xia Y-F, Xue Y, Wu J (2017) Studies on stability and capacity for long-life cycle performance of Li(Ni0.5Co0.2Mn0.3)O2 by Mo modification for lithium-ion battery. J Power Sources 358:1–12
30. Hu SK, Cheng GH, Cheng MY, Hwang BJ, Santhanam R (2009) Cycle life improvement of ZrO_2-coated spherical $LiNi_{1/3}Co_{1/3}Mn_{1/3}O_2$ cathode material for lithium ion batteries. J Power Sources 188:564–569
31. Wang J, Du C, Yan C, He X, Song B, Yin G, Zuo P, Cheng X (2015) Al_2O_3 coated concentration-gradient Li $[Ni_{0.73}Co_{0.12}Mn_{0.15}]O_2$ cathode material by freeze drying for long-life lithium ion batteries. Electrochim Acta 174:1185–1191
32. Ke D, Xie H, Hu G, Peng Z, Cao Y, Fan Y (2016) Enhancing the thermal and upper voltage performance of Ni-rich cathode material by a homogeneous and facile coating method: spray-drying-coating nano-Al_2O_3. ACS Appl Mater Interfaces 8:17713
33. Zhou Y, Lee Y, Sun H, Wallas JM, George SM, Xie M (2017) Coating solution for high-voltage cathode: AlF_3 atomic layer deposition for free-standing $LiCoO_2$ electrodes with high energy density and excellent flexibility. ACS Appl Mater Interfaces 9:9614–9619
34. Yang C, Zhang X, Huang M, Huang J, Fang Z (2017) Preparation and rate capability of carbon coated $LiNi_{1/3}Co_{1/3}Mn_{1/3}O_2$ as

cathode material in lithium ion batteries. ACS Appl Mater Interfaces 9:12408–12415
35. Wang JH, Wang Y, Guo YZ, Ren ZY, Liu CW (2013) Effect of heat-treatment on the surface structure and electrochemical behavior of $AlPO_4$-coated $LiNi_{1/3}Co_{1/3}Mn_{1/3}O_2$ cathode materials. J Mater Chem A 1:4879–4884
36. Su Y, Cui S, Zhuo Z, Yang W, Wang X, Pan F (2015) Enhancing the high-voltage cycling performance of $LiNi_{0.5}Mn_{0.3}Co_{0.2}O_2$ by retarding its interfacial reaction with electrolyte by atomic layer deposited Al_2O_3. Zeitschrift Für Physik C Part Fields 7:25105–25112
37. Guo X, Cong LN, Zhao Q, Tai LH, Wu XL, Zhang JP, Wang RS, Xie HM, Sun LQ (2015) Enhancement of electrochemical performance of $LiNi_{1/3}Co_{1/3}Mn_{1/3}O_2$ by surface modification with MnO_2. J Alloys Compd 651:12–18
38. Ma Z, Shao G, Fan Y, Wang G, Song J, Shen D (2016) Construction of hierarchical α-MnO_2 nanowires@ ultrathin δ-MnO_2 nanosheets core-shell nanostructure with excellent cycling stability for high-power asymmetric supercapacitor electrodes. ACS Appl Mater Interfaces 8:9050–9058
39. Ma Z, Shao G, Fan Y, Feng M, Shen D, Wang H (2017) Fabrication of high-performance all-solid-state asymmetric supercapacitors based on stable α-MnO_2@$NiCo_2O_4$ core-shell heterostructure and 3D-nanocage N-doped porous carbon. ACS Sustain Chem Eng 5:4856–4868
40. Ma Z, Jing F, Fan Y, Hou L, Su L, Fan L, Shao G (2019) High-stability MnOx nanowires@C@MnOx nanosheet core–shell heterostructure pseudocapacitance electrode based on reversible phase transition mechanism. Small 15:1900862
41. Cheng F, Su Y, Liang J, Tao Z, Chen J (2014) MnO_2-based nanostructures as catalysts for electrochemical oxygen reduction in alkaline media†. Chem Mater 22:898–905
42. Yin X, Dong H, Sun G, Yang W, Song A, Du Q, Su L, Shao G (2017) Ni–MoS2 composite coatings as efficient hydrogen evolution reaction catalysts in alkaline solution. Int J Hydrog Energy 42:11262–11269
43. Dose W, Donne S (2011) Kinetic analysis of Î³-MnO thermal treatment. J Therm Anal Calorim 105:113–122
44. Xia H, Lai MO, Lu L (2010) Nanoflaky MnO_2/carbon nanotube nanocomposites as anode materials for lithium-ion batteries. J Mater Chem 20:6896–6902
45. Tu F, Wu T, Liu S, Jin G, Pan C (2013) Facile fabrication of MnO_2 nanorod/graphene hybrid as cathode materials for lithium batteries. Electrochim Acta 106:406–410
46. Brenet J, Faber P (1979) Conductivity measurements on pure and mixed metal dioxides ☆. J Power Sources 4:203–213
47. Lee J, Newnham C, Tye F (1973) Energetics of water desorption from a γ-manganese dioxide. J Colloid Interface Sci 42:372–380
48. Ren D, Shen Y, Yang Y, Shen L, Levin BD, Yu Y, Muller DA, Abruña HcD (2017) Systematic optimization of battery materials: key parameter optimization for the scalable synthesis of uniform, high-energy, and high stability $LiNi_{0.6}Mn_{0.2}Co_{0.2}O_2$ cathode material for lithium-ion batteries. Acs Appl Mater Interfaces 9:35811–35819
49. Li X, Liu J, Banis MN, Lushington A, Li R, Cai M, Sun X (2014) Atomic layer deposition of solid-state electrolyte coated cathode materials with superior high-voltage cycling behavior for lithium ion battery application. Energy Environ Sci 7:768–778
50. Reed J, Ceder G, Ven AVD (2001) Layered-to-spinel phase transition in LiMnO. Electrochem Solid-State Lett 4:A78
51. Gu M, Belharouak I, Zheng J, Wu H, Xiao J, Genc A, Amine K, Thevuthasan S, Baer DR, Zhang JG (2013) Formation of the spinel phase in the layered composite cathode used in Li-ion batteries. ACS Nano 7:760–767
52. Wang L, Zhao J, He X, Gao J, Li J, Wan C, Jiang C (2012) Electrochemical impedance spectroscopy (EIS) study of LiNi1/3Co1/3Mn1/3O2 for Li-ion. Batteries Int J Electrochem Sci 7:345–353